

COMPOSITIONS OF C/H SYSTEMS AT HIGH TEMPERATURES.  
SHOCK TUBE DATA AND A THEORETICAL ANALYSIS.

S. H. Bauer, R. E. Duff<sup>\*</sup>, M. Cowperthwaite, and W. Tsang  
Department of Chemistry, Cornell University, Ithaca, New York  
and

<sup>\*</sup>University of California, Los Alamos Scientific Laboratory,  
Los Alamos, New Mexico

## INTRODUCTION

During the past seventy-five years, numerous experiments have been performed on the pyrolysis of hydrocarbons, of both low and high molecular weights. In reports describing these investigations, there are listed a large variety of products so obtained. It was readily demonstrated that the pyrolytic processes are very complex, involving numerous inter-conversions of the hydrocarbons. The rates of decomposition of the initial material and that of the production of the host of products depended on many factors. Two general types of techniques have been used for the kinetic studies. In the fixed-volume experiments, the material was subjected to modest temperatures for relatively long contact times. Pressure changes were noted, and after quenching the residues were analyzed. Somewhat later, flow techniques were introduced, and the operating temperatures were raised to the neighborhood of 1000°K. with a corresponding decrease in contact time. Along with the inherent analytical difficulties due to the complexity of the reactions, there appeared a disturbing problem. Both in the fixed-volume and the flow through a hot tube experiments, the heterogeneous reactions induced by the heated walls could not be readily separated from the homogeneous reactions which were of primary interest. Also, the gas samples could not be uniformly heated due to limitations on the rate of heat transfer from the walls. It has been generally established that the decomposition is initiated by rupture of carbon-hydrogen and carbon-carbon bonds. The radicals thus produced initiate chains which produce the complex mixture of products. Further details may be found in numerous papers and books<sup>1,2,3</sup>.

The chemical properties of the radicals produced in the pyrolytic reactions are not only of direct interest to those concerned with the behavior of organic compounds but also constitute essential information to those who would analyze the course of the hydrocarbon decomposition. During the past twenty years, much effort has been expended in the study of gaseous radicals. Generally, these have been produced by photochemical dissociation of selected gases; their chemical properties have been deduced from the subsequent reaction of the radicals with the ambient gas. These techniques have been extended to cover an appreciable range in radical type, temperature, and medium.<sup>4,5,6,7</sup> Production via photochemical processes is often limited by the light intensity available, so that the concentration of radicals generated is quite small. Use of intense photoflashes<sup>8,9</sup> and electrical discharges<sup>10</sup>

permits the production of appreciable concentrations. We thus anticipate extended current activity in the investigation of the chemical properties of radicals. Were this information available now, it would mitigate but not solve the pyrolysis problem, since it is abundantly clear that the pyrolytic processes in hydrocarbons exposed to temperatures of 1000°K. or below are complex because many competing rates are involved.

During the past decade, a new technique has been developed, the utilization of shock tubes for chemical kinetic investigations. The upper temperature range is easily extended to about 5000°K. Shock tube heating has the added attractive features that the gas is homogeneously and rapidly heated to a uniform temperature (in less than a microsecond) and the reactions occur so rapidly that there is no time for confusion by a heterogeneous process which may occur on the walls. During a temperature pulse, the time required to attain a temporary state of equilibrium may be 100 microseconds to several milliseconds. Hence, these kinetic studies require the development of specific analytical methods, which have microsecond resolution. The single-pulse technique<sup>11</sup> avoids the necessity for such rapid and specific analytical procedures. The shocked gases are rapidly quenched after a selected dwell time of (1-5) milliseconds and the residual gases analyzed by conventional techniques. The quench rates obtained,  $(1-4) \times 10^5$ °K/sec., are barely adequate for terminating those steps in the complex mechanisms which have appreciable activation energies. Atom abstractions, free-radical rearrangements, and recombinations continue. Hence, the interesting product distributions which have been reported must be interpreted with care.<sup>12,13,14,15,16,17,18,19</sup> As an example, one may cite the range of 'first-order' decomposition rate constants reported for the pyrolysis of methane. The early hot tube experiments at around 1000°K. gave an activation energy of 79 kcal.<sup>20</sup>; then in succession, shock tube values (for the temperature range 1200-2100°K.) were reported which ranged from 85 kcal.<sup>14</sup> to 93 kcal.<sup>17</sup> to 101 kcal.<sup>18</sup> There were differences in the magnitudes of the rate constants (factors of 3 to 5), such that were one to draw the best straight line through all the shock tube data the deduced activation energy would be about 10<sup>4</sup> kcal. It is presumed that the primary step produces CH<sub>3</sub> radicals, and the product distribution following the quench depends on the height and width of the temperature pulse to which the methane was subjected; the amount of acetylene increases with a rise in temperature, the yield of ethylene passes through a maximum, and ethane is found in small amounts only.

The higher hydrocarbons, although studied in many laboratories, have not been as extensively investigated as methane. A shock tube pyrolysis of ethane<sup>18</sup> (1059-1410°K.) indicated a decomposition rate which was first order in the reactant, with an activation energy of 60 kcal. The primary step is presumed to be the fission of the C-C bond to produce two CH<sub>3</sub>'s. This is followed by a sequence of free-radical reactions. There are a number of serious loopholes in the proposed mechanism, not the least being that the proposed rate constant for the dissociation of ethane is inconsistent with the measured rate constant for the association of two methyl radicals.<sup>21</sup> The products found after the quench were ethylene, acetylene, methane, hydrogen, and some 1,3-butadiene. The pyrolysis of ethylene<sup>19</sup> was similarly investigated; acetylene and 1,3-butadiene were the principal products, the acetylene being formed via a first-order step with an activation

energy of approximately 46 kcal., while the butadiene was generated via a net second-order reaction. The proposed mechanism is that  $C_2H_4 \rightarrow C_2H_4^* \rightarrow C_2H_2 + H_2$ .

The large variety of products and the often conflicting conclusions deduced from different experiments suggest that the reported differences are not due to poor technique; rather, they reflect the sensitivity of these studies to different experimental conditions. Since the pyrolysis reactions follow very complex mechanisms, small differences in experimental parameters selectively favor different controlling steps, and the differences in rates and product distributions are thereby considerably amplified. This point of view has been corroborated by our studies of the C/H system.

In the experiments performed in our laboratory<sup>22</sup>, one of the objectives has been the search for conditions under which the pyrolytic process may prove relatively simple. It was presumed that the higher the temperature the simpler the species which must be considered. In our study of the pyrolysis of ethylene over the temperature range 3000-4000°K., we followed spectrophotometrically the changes which occur in the gas. Timewise, the method has adequate resolution, but it is not sufficiently distinctive to permit identification of many of the species which nonetheless are present under these conditions. Principally, we used the characteristic absorption by  $C_2$  as a means of determining its population in the  $v = 0$  vibrational state of the  $^3\Pi_u$  electronic state. Two postulates were made in setting up this experiment. (a) With regard to translation, rotation, and vibration of all the molecular species involved, equilibrium is rapidly attained in the shock front, in a time small compared to the changes in concentration of  $C_2$ , and (b) equilibrium is not attained with regard to the precipitation of carbon even at the end of our observation time (which is of the order of 1 millisecc.). The latter may be justified on the basis of data reported by Kistiakowsky and confirmed in other laboratories<sup>23</sup>.

The computations described below provide a glimpse of the complex kinetics which may be operative by ascertaining the equilibrium compositions of systems containing carbon and hydrogen which are being approached through the involved kinetic processes. Since the variety of molecular fragments which are conceivable is enormous, the equilibrium composition may serve to point to those species which are present in appreciable concentrations as the dominant ones in propagating chains. One might anticipate that in the long history of the study of hydrocarbons such computations would have been made. Only two attempts have been described recently<sup>24,25</sup>, and in neither did the authors consider the full range of species required to provide an adequate analysis. Furthermore, in the more general computations described by Kroepelin and Winter<sup>24</sup>, questionable values were used for the thermodynamic functions of those species which were included.

#### KINETICS OF PRODUCTION OF $C_2$ FROM ETHYLENE

Shock tube studies reported below were made in a conventionally instrumented shock tube, 1-1/2" in diameter. The driver length was 35.5", and the sample section was 129.3". The driver gas (hydrogen) ranged in pressures from 5 to 15 atm. The driven gas consisted of a mixture of 92% argon and 8% ethylene. The impurity level in the

ethylene as established by mass spectrometric analysis was less than 0.4%. It was particularly desirable in these studies to avoid contamination by oxygen; we estimate that the oxygen impurity was less than 0.1%. Shock speeds of the forward-moving wave were measured by means of narrow platinum film gauges supported on pyrex rods mounted flush with the inside of the shock tube. These speeds ranged from 1.30 to 1.55 mm. per microsecond.

A schematic of the experimental arrangement is shown in Fig. 1. To record the changes in the absorption spectrum of the sample which had been subjected to a shock, two types of configurations were used. In the first, a continuum of wave lengths was generated by discharging a condenser (1.0  $\mu$ f, 10 KV) through a small quartz tube through which argon was flowing at a pressure of approximately 50 mm. Hg.<sup>28</sup> This produced an intense emission which initially rose sharply and fell to half of the peak intensity in about 10 microseconds. The light which passed through the shocked gas was picked up by a mirror and sent to a grating spectrograph (Fig. 1, right corner) in which a camera was substituted for the photomultiplier tube. By delaying the source trigger pulse, the argon continuum was generated at predetermined times after passage of the reflected shock past the observation ports. The transmission spectra were then photographed (at 16 A° per millimeter dispersion) over the range  $\lambda$ 3900 to  $\lambda$  6000, thus providing a record of the absorption intensity as a function of wave length at specified intervals after initiation of the reaction. The photographs show a general absorption which is fairly uniform over the longer wave lengths but increases rapidly below some critical wave length which depends on the time interval. Upon this background, there was clearly superposed a well developed Swan band system. As far as we can tell, no measurable absorption due to C<sub>2</sub> was discernable at  $\lambda$  4050, although there are indications from preliminary experiments that a small amount of absorption due to this species did appear during the higher temperature runs.

To study the rate of appearance of C<sub>2</sub>, a characteristic source was placed at the position indicated in Fig. 1. The light was split with a half-silvered mirror, so that the JACO monochromator phototube monitored the intensity of a small wave length interval near  $\lambda$ 5165, while the small grating spectrograph with the phototube attachment monitored the intensity of the mercury line at  $\lambda$ 5460. The characteristic source was generated by a discharge of a 2  $\mu$ f condenser at about 12 KV through a tube filled with butane, helium, and mercury. The outputs of the two 1P28 photocells were led to a 100 KC electronic switch, so that the relative absorption by the shock sample of the two characteristic emission regions was displayed on one oscilloscope record. The optical window was 0.5 A° wide and set at the band head of the (0,0) band of the  $^3\pi_g \rightarrow ^3\pi_u$  transition for C<sub>2</sub>. The percent absorption recorded in this manner is thus a measure of the population of the C<sub>2</sub> species present in the zero vibrational level of the  $^3\pi_u$  state. Because a continuum absorption is superposed on the characteristic absorption, a correction for the former should be made. It was convenient to monitor the background absorption at the  $\lambda$ 5460 mercury line. The error introduced by the displacement of 300 A° is of secondary significance, since the essential kinetic data were derived during the induction period, when the background absorption was negligible. Since the populations of the lower states for these lines change with the temperature, a correction was made in reducing the percent absorption to relative concentration.

Fig. 2 is a sketch of a typical reduced oscilloscope trace. The solid line is the intensity recorded at the  $C_2$  band head, and the dashed line is that recorded at the  $\lambda 5460$  mercury line. The characteristic features of these curves which will be subjected to analysis are indicated in the figure. One may add that after the induction time  $\tau$  the difference between the dashed and solid curve is very nearly constant for periods up to one millisecond, indicating that a steady-state concentration in  $C_2$  was reached at a time prior to the beginning of the continuum absorption at this wave length.

Although an absolute calibration for the concentration of  $C_2$  is not available, since no reliable  $f$  value for this band is known, one may nevertheless determine relative rates of production from the initial slope of the oscilloscope trace. To deduce the order of the reaction for the production of  $C_2$ ,  $d/dt (\log I_0/I)_1$  was plotted vs.  $\log p_3$  (the density of the shocked gas in the reflected shock region). The data are consistent with a first-order rate of production of  $C_2$  (with respect to  $p_3$ ) during the early stage of the pyrolysis. It follows

$$\left(\frac{dC_2}{dt}\right)_1 = \frac{2.3}{\langle \mu \rangle} \frac{d}{dt} (\log I_0/I)_1 = k_1 p_3$$

The activation energy for the production rate constant  $k_1$  may be obtained, as in Fig. 3, from a plot of

$$\log \left[ \frac{1}{p_3} \frac{d}{dt} (\log I_0/I)_1 \right] \text{ vs. } 1/T.$$

The deduced value for the activation energy is  $68 \pm 10$  kcal., obtained from the best visually estimated straight line through all the points.

From traces such as Fig. 2, it was evident that a steady-state concentration of  $C_2$  was attained after a time varying from 50 to 300 microseconds. The approach to a limiting value (designated  $D_{ss}$ ) implies that some process removes  $C_2$ , eventually at a rate equal to that of production. It was demonstrated that the order of the scavenging reaction is close to unity and that the rate for removal of  $C_2$  proceeds with essentially zero activation energy.

Attention is called to another feature which appears in the oscilloscope traces. In Fig. 2, an induction time ( $\tau$ ) was defined as the first appearance of absorption, monitored at the  $\lambda 5460$  mercury line. This background absorption is presumed to be due to large molecular-weight polyaromatic or conjugated high molecular fragments. We infer from qualitative observations that the length of the induction period decreases with decreasing wave length, and in the ultraviolet the background absorption can be detected even in the incident shock region. With the passage of time, the edge of the intense absorption region shifts toward the red, and the entire level of absorption increases. We estimate from the total absorption curve recorded at 300 microseconds after passage of the shock that the dominant species are polyaromatic nuclei which contain on the average four condensed aromatic rings or their equivalent in the form of a highly conjugated polyene chain. The induction time multiplied by the reflected shock density appears to be constant for shock temperatures above  $3000^\circ\text{K}$ .

POSSIBLE MECHANISM FOR THE FORMATION OF  $C_2$ 

Since the data have been gathered for the reflected shock, the question arises as to whether the incoming shock had processed the material with which the shock tube was filled. Between the passage of the incoming and reflected shocks, no detectable quantity of  $C_2$  was generated, nor was there any absorption apparent in the visible. Nonetheless, the incoming shock had processed the ethylene and had produced some new products, since a small amount of absorption was detected in the limit of our working region in the ultraviolet. For the elapsed time (between the forward and reflected shocks at the position of our observation port) of the order of 300 microseconds, a major portion of the ethylene (perhaps as much as 80%) must have been converted to acetylene plus hydrogen. This estimate is based on the first-order rate constant for the molecular reaction  $C_2H_4 \rightarrow C_2H_4^* \rightarrow C_2H_2 + H_2$ .<sup>19</sup>

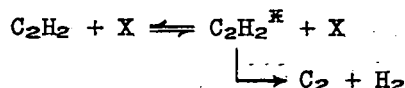
$$-\frac{d(C_2H_4)}{dt} = k_2 (C_2H_4) ; \quad \log k_2 = 8.87 - \frac{10,150}{T}$$

The resulting mixture is then heated a second time by the reflected shock to produce the following 'initial' composition (indicated by the symbol  $\rho_3$ ) in the reflected shock front. At  $t = 0$ ,

$$\rho_3 = \frac{np_3}{RT_3} [2 x_{H_2} + 26 x_{C_2H_2} + 28 x_{C_2H_4} + 40 x_{Ar}]$$

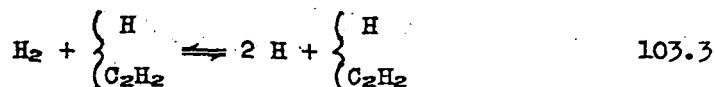
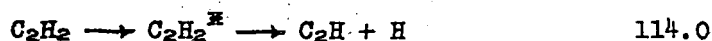
wherein the mole fraction of the argon ( $x_{Ar}$ ) by far dominates the magnitude in the bracket.

Since our results indicate a pseudo-unimolecular rate of appearance for  $C_2$  in the  $^3\pi_u$  state, one might be tempted to write



However, this cannot be the process we observe. In the first place, the activation energy expected for this step is 140 kcal., compared with the experimental value of 70 kcal. Secondly, due to the spin conservation restrictions, the  $C_2$  which is generated in such a step would of necessity be in a  $^1\Sigma$  state, since both the reactant (acetylene) and the second product formed ( $H_2$ ) are in singlet states. It may well be that some acetylene decomposes in this manner to produce  $C_2$  molecules in the ground  $^1\Sigma_g^+$  state, but the collision-induced transition to the  $^3\pi_u$  state would be expected to require many molecular encounters and take considerable time. One must conclude that  $C_2$  was produced in the  $^3\pi_u$  state via a chain reaction, that the over-all initial production rate was pseudo first order, and that during the subsequent pyrolysis a steady state was reached wherein the  $C_2$  was consumed as rapidly as it was produced. We shall propose a combination of reactions which form a chain for which one would anticipate an activation energy of around 70 kcal.

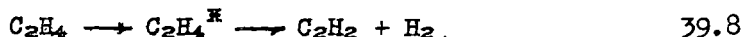
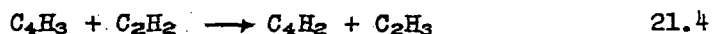
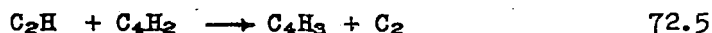
## Initiation:

 $\Delta H_0^\circ$ , kcal.

## Enhancement of the carrier:



## Propagation:



The controlling activation energy in the propagation sequence should be of the order of 72 kcal., as estimated for  $\Delta H_0^\circ$ . This mechanism is consistent with the observations made in our laboratory and the data reported in the literature. However, it is evident that there are many other possible chains. Furthermore, there must be many steps involving the transfer of H atoms which require small activation energies; these reach a steady-state condition rapidly and in effect attain a local equilibrium. Before attempting to select between possible alternate mechanisms and an analysis of the details of the termination steps, we consider it worthwhile to answer the fundamental question: what is the composition of the system toward which this kinetic condition is drifting?

## ESTIMATION OF MOLECULAR PARAMETERS OF C/H FRAGMENTS:

In our first attempt<sup>22</sup> to compute the equilibrium composition of C/H systems at elevated temperatures, we considered 43 species. This and subsequent analysis showed that particularly for carbon-rich systems the list was incomplete and that a second approximation was necessary. Therefore, it is our objective to estimate the heats of formation and the molecular parameters, such as the moments of inertia and vibrational frequencies, with sufficient certainty to permit the computation of the thermodynamic functions in the ideal gas state as they depend on the temperature, for the large number of low-molecular weight species consisting of carbon and hydrogen. The temperature range we intend to cover is 500-5000°K. The species considered are listed in Table I. The molecular parameters and heats of formation were taken from the literature wherever available. A considerable amount of guessing was needed to complete the list. Estimates were made with the help of analogies, bond dissociation energies derived from kinetic data, and mass spectrometer appearance potentials, with due allowance for resonance stabilization.

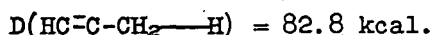
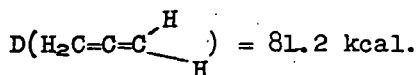
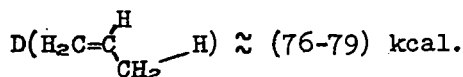
In Table I, we have also listed values for the heats of formation. Those shown in parentheses are based directly on experimental measurements, whereas the ones given in square brackets were estimated by means of an empirical theory. Thus, experimental values which link two states (for example,  $C_3H_3 \rightarrow C_3 + 3 H$ ) were divided into unit steps ( $C_3H_3 \rightarrow C_3H_2 + H \rightarrow C_3H + 2 H \rightarrow C_3 + 3 H$ ) on the basis of empirically assigned parameters. The justification for this procedure and the consequent deduction of structures and vibrational frequencies are given in detail elsewhere. It is essential to recognize that the best guess no matter how tenuous its basis is by far a better approximation than the omission of that species from the computation, since the latter merely implies that an excessively large value has been arbitrarily assigned to its heat of formation. The reasons for the omission of some species (footnote to Table I) will become evident from the inspection of the computations and comparison of estimated heats of formation for these species with the corresponding isomers which were included. Typical results based on computations of the equilibrium compositions for various C/H ratios are presented in the following section. It can be shown that all the isomers of comparable stability must be included in the solutions of the simultaneous equations which give the composition at equilibrium. Indeed, this is even so if the isomers have the same thermodynamic functions; however, under this simplifying condition, a contraction can be made so that the sum of the concentrations of all the closely similar isomers may be obtained by the use of an effective equilibrium constant.

It is well known that equilibrium constants can be calculated for all possible reactions between any given set of species when for each species the moments of inertia, symmetry number, electronic degeneracy, vibrational frequencies, the corresponding degeneracies, and heat of formation at 0°K. are known. It should be realized that the equilibrium constants are more sensitive to changes in some of the molecular parameters than others. Because of their weighting in the partition function, the vibrational frequencies need be known only roughly. It is also fortunate that for these C/H species one has to consider a narrow range of interatomic distances, so that the rotational contributions to the partition functions may be computed with acceptable accuracy. For many molecules, the heats of formation may be estimated at best to within several kilocalories; consequently, this parameter exercises a maximum influence on the computations. However, for the high molecular-weight species containing more than two hydrogen atoms, it is not so sensitive a variable, because these fragments will be present in very small amounts. Changes even in an order of magnitude in their concentrations will have a negligible effect on the equilibrium amounts of the prevalent species.

In estimating the heats of formation, we had to postulate reasonable molecular structures and assign to them electronic configurations. Full use was made of experimental values to provide empirical bond dissociation energies and correction factors ascribed to changes in the basic configurations due to hybridization, delocalization, and other nonbonded interactions. This procedure led to a self-consistent set of values for the heats of formation, the interatomic distances, and the fundamental vibrational frequencies. To check this procedure in a number of cases, we computed the enthalpy changes to be expected for specified dissociations and compared them with experimentally available enthalpy increments for the corresponding steps. For some molecular fragments, the heats of formation were estimated following independent paths and checked against each other.

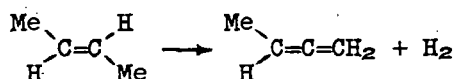


An illustration of the procedures evolved for estimating heats of formation is the set of values deduced for crucial parameters in the  $C_3$  sequence. The changes in electron configurations associated with the successive removal of hydrogen atoms from propene to generate  $C_3$  are indicated in Fig. 4. Experimental values are available for

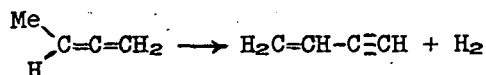


Consider the first dissociation shown in Fig. 4. The observed value (78 kcal.) may be expressed as the sum  $(98 + a - \gamma)$ , where  $\gamma = 23.1$  kcal. denotes the energy gained by the nonbonded interactions present in the  $H_2C-CH-CH_2$  radical. To remove the second hydrogen atom, one must expend 104 kcal. (ethylenic C-H) and  $\gamma$  kcal. (stabilization energy) but regains  $a$  kcal., which leads to a BDE of 65.3 kcal. This compares favorably with 64.4 kcal. deduced by taking direct differences between experimental quantities. Similar arguments for the production of the  $CH_2-C\equiv CH$  radical from methyl acetylene and allene lead to  $\epsilon = 20.5$  kcal. and  $\delta = 22.8$  kcal., respectively. These and other similarly deduced parameters were used to evaluate BDE's for analogous steps in the higher  $C_n$  sequences.

As a gauge of the reliability of this semi-empirical method, consider the reaction



The estimated value for its  $\Delta H_0^\circ$  is 143.8 kcal., compared with the experimental value of 143.0 kcal. For the reaction



the estimated  $\Delta H_0^\circ$  is 135.6 kcal., while the experimental value is 136.5 kcal. The self-consistency of the method may be judged by comparing estimates of the heats of formation of radicals each generated via several independent paths. Thus, for  $H_2\dot{C}-CH=C=CH_2$ ,  $(\Delta H_{0f}^\circ)_{\text{est}} = 66.8, 67.7, \text{ and } 67.7$  kcal; for  $H_2C=\dot{C}=CH_2$ ,  $(\Delta H_{0f}^\circ)_{\text{est}} = 71.7, 70.8, 70.8, 71.7$  kcal; for  $H_2C=C-\dot{C}\equiv H$ ,  $(\Delta H_{0f}^\circ)_{\text{est}} = 103.9 \text{ and } 101.1$  kcal. Further examples are illustrated in Table II; the processes correspond to the steps illustrated in Fig. 5.

The compilation of bond lengths by Costain and Stoicheff<sup>27</sup> for many C/H compounds shows that the C-C and C-H bond lengths for a given bond environment are remarkably constant in different molecules.

Since we have postulated the electronic structures of the unknown species, justifiable estimates of bond lengths and bond angles can be made by comparisons and interpolation with the known bond types listed by these authors.

Although it is well appreciated that in each normal mode all the atoms participate, the  $(3n-6)$  unknown frequencies may be assigned to a sufficient accuracy by subdividing the vibrations into classes associated primarily with bond stretching, bond bending, and skeletal motions. Comparison of each vibration with a similar type in molecules whose frequencies are known led to reasonable frequencies. We often assumed that many of the frequencies of a radical produced by the removal of a hydrogen atom will be those of the parent molecule minus the frequencies associated with the C-H bond broken, namely one C-H stretching and two C-H bending frequencies. The correlation of the frequencies of a radical with those of its parent requires consideration of changes in some force constants and in the reduced masses. The hydrogen atom is so light that for most of the compounds in Table I only changes in carbon atom hybridization appreciably affect the molecular frequencies due to corresponding changes in force constants. The deduced frequency change for C-C bonds follows from the assumed changes in hybridization. Skeletal bending frequencies are the most difficult to predict, because they correspond to motions involving the entire molecule. However, these are usually of the order of  $300\text{ cm}^{-1}$ , and errors in the partition functions due to incorrect estimates can be neglected because of the high temperatures involved in the computation of equilibrium compositions.

Less error is expected in the estimation of C-H frequencies. The hydrogen atoms may be regarded as oscillating against an infinitely large mass; the vibrational frequency depends practically only on the force constant for the C-H bond and will be approximately constant for species with the carbon atom in a given state of hybridization.

The free energies, as dependent on the temperature, were taken from the literature wherever they were available. This was the case for the stable species in the low-temperature regime (up to  $1500^\circ\text{K}$ ). The numerical values as given in the NBS tables were plotted on a large scale and twelve to fifteen values read between the temperature range  $500$ - $1500^\circ\text{K}$ . They were then fitted by least squares to the polynomial form

$$\frac{F_T^\circ - H_0^\circ}{RT} = a (1 - \ln T) - bT - c/2 T^2 - d/3 T^3 - e/4 T^4 - k$$

$$\frac{H_T^\circ - H_0^\circ}{RT} = a + bT + cT^2 + dT^3 + eT^4$$

Since the same coefficients appear in the expression for the enthalpy and free energy, the magnitude of  $k$  may be computed for each temperature; the value used was the average over the equally spaced temperature points. To obtain the corresponding fit coefficients for the stable species over the upper temperature, the usual ideal gas, rigid rotor, and simple harmonic oscillator approximations were made. The thermodynamic functions were computed following an IBM 704 code written by

L. R. Sitney<sup>28</sup>. The same procedure was followed for the unstable species; the computed functions were again least-square fitted to the indicated polynomial form. We thus have two sets of thermodynamic fit coefficients suitable for the two ranges indicated. Details of the computations (the basis for decisions as to the nature of the ground electronic states, the presence and location of low-lying electronic states, corrections for internal rotation, etc.) will be presented in another publication.

## THE EQUILIBRIUM COMPOSITIONS

In the computation of equilibrium compositions, we considered two cases. The first and most extensive set of graphs was obtained under the assumption that at the specified pressure and temperature equilibrium was attained for all the species listed, except with respect to the presence of solid carbon. The second set of computations will be performed under the assumption of complete equilibrium including the presence of solid carbon. Although the first case seems artificial, it is significant kinetically. Such a restriction correctly describes a situation in many shock tube and detonation experiments<sup>29</sup> (carbon-rich mixtures) during the intermediate stages of reaction. Since the precipitation of graphite (in highly irregular crystalline form) must await the prior formation of nuclei, the gaseous components attain a pseudo-equilibrium which lasts sometimes for hundreds of microseconds before particles appear. The following ranges in parameters were covered:  $C/H = 1/10, 1/4, 1/2, 1, 1\frac{1}{2}, \text{ and } 1\frac{1}{2}$ ;  $p = 10, 1, \text{ and } 0.1$  atm;  $T = 500\text{-}5000^\circ\text{K.}$  in two intervals,  $500\text{-}1600^\circ\text{K.}$  and  $1500\text{-}5000^\circ\text{K.}$

A question remains as to where one may properly terminate the list of species to be included in the equilibrium computation. Evidently, the answer is based on the rate of convergence of the concentrations to a limiting value in the sequence of successive approximations in which more and more species are added. We have found this convergence depends sensitively on the  $C/H$  ratio and on the temperature. A comparison of the concentrations deduced in our first computation with the present values indicates that values for the major species for the low  $C/H$  compositions were converging rapidly, but that was not the case for the high  $C/H$  compositions at the low temperatures.

In performing the computations described below, it is essential that all the isomers be included. Only the isomers which have heats of formation considerably larger than those covered by the computations or such species the dissociations of which are greatly favored by a large entropy increase at the cost of a small enthalpy increment may be omitted.

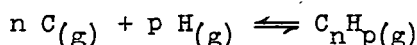
For a sequence of temperatures and a specified total pressure, the equilibrium (no solid carbon allowed) partial pressures were computed by an IBM 704 program set up by W. Fickett and modified by one of the authors (R.E.D.). Typical graphs are shown in Figs. 6-13; only the upper 8 decades of the partial pressures have been plotted. The 58 species (for which the thermodynamic functions were inserted in the simultaneous equations) were divided into groups on the basis of their hydrogen content. A complete set of such graphs is shown for  $C/H = 1/2$ ,

but a few selected curves for other C/H ratios were included to demonstrate the effect of change in that parameter on the partial pressures. Variation of the total pressure slightly modified the partial pressures, as expected from 'mass law' considerations.

A general inspection of the curves plotted leads to two important conclusions:

(a) For temperatures above 1500°K., numerous molecular fragments attain significant concentrations. Insufficient attention has been given to the presence of the  $C_nH$  and  $C_nH_2$  fragments in the pyrolysis of hydrocarbons. The fact that these and others appear prominently in our plots underlines the importance of including as complete a set as is possible in the computations of the equilibrium partial pressures.

(b) For  $C_nH_p$ , those species which have the same p's show on the whole similar trends as a function of temperature. Consider the general equilibrium.



$$K_{eq}(T) = \frac{(C_nH_p(g))}{(C_g)^n (H_g)^p} = e^{-\Delta F_T^\circ/RT}$$

$$\ln (C_nH_p(g)) = n \ln (C_g) + p \ln (H_g) - \Delta F_T^\circ/RT$$

Define  $G_1 \equiv \left(\frac{F_T^\circ - H_C^\circ}{RT}\right)_1 + \left(\frac{\Delta H_{Of}^\circ}{RT}\right)_1$ ; this is known for all the species considered.

$$\ln (C_nH_p(g)) = n [\ln(C_g) + G(C_g)] + p [\ln(H_g) + G(H_g)] - G(C_nH_p)$$

For any specified C/H ratio, pressure and temperature, the partial pressure at equilibrium of monatomic carbon gas and monatomic hydrogen is fixed. For any species,  $\ln (C_nH_p)$  is linearly dependent on  $n$  and  $p$  and on the magnitude of the  $G(C_nH_p)$  function which expresses the thermodynamic potential of that species at that particular temperature. The observation that the partial pressures of  $C_nH_p$  species for equal  $p$  have roughly parallel temperature dependences suggests that the  $G(C_nH_p)$  function is sensitive to the magnitude of  $p$  but varies gradually and regularly with  $n$ . Trends of composition with C/H ratio and temperature are given below.

(c) The  $C_n$  sequence: as  $T$  increases above 2000°K., the concentrations of all  $C_n$ 's increase. At the highest temperatures, the relative pressures decrease with  $n$ . Between 2000-2500°K.,  $C_3$  dominates. Below 3500°K.,  $(C_5) > (C_4)$ ,  $(C_7) > (C_6)$ . Per mole of carbon, the sum of the concentrations of the  $C_n$  species increases as the C/H ratio increases, as expected.

(d) The  $C_nH$  system: the concentration of CH is unexpectedly small. Up to 3000-4000°K. (depending on the C/H ratio), the dominant species are  $C_3H$  and  $C_4H$ ; at higher temperatures,  $C_2H$  dominates. Note also that  $C_6H > C_5H$ ,  $C_9H > C_8H$ . The absolute concentrations are very sensitive to the C/H ratio.

(e) The  $C_nH_2$  system: the curves recorded for  $C/H = 1/2$  are typical. The concentration of these species goes through a maximum between 1500-2000°K. As is well known from the experiments mentioned above, the partial pressure of acetylene rises rapidly as  $T$  approaches 1000°K. At higher temperatures, its partial pressure declines gently and is overtaken by  $CH_2$  only for  $T > 4000^\circ K$ . Next in prominence is diacetylene.

(f) The  $C_nH_3$  and  $C_nH_5$  systems: these species go through a maximum at a temperature which depends on the  $C/H$  ratio, in the vicinity of 1500°K. As the proportion of hydrogen increases, the concentration of species with lower  $n$  increases.  $C_3H_5$  is most prominent except for systems which have a small amount of hydrogen. This is a consequence of the symmetry in electron distribution which the molecule possesses; resonance provides it with a high relative stability. Above 2500-3000°K.,  $CH_3$  dominates in concentration; it is followed closely by  $C_2H_3$  and  $C_3H_3$ .

(g) The  $C_nH_4$  system: on this graph, the concentrations of molecular and atomic hydrogen have also been included. These behave as expected for the equilibrium  $H_2 \rightleftharpoons 2 H$ . The hydrocarbons which are usually thought of as being stable rapidly decline in abundance for temperatures above 1500°K. and attain partial pressures below  $10^{-3}$  as  $T$  approaches 2000°K; their relative concentrations decrease in magnitude with increasing  $n$ . In general, for the stable species, the sum of their concentrations increases as the  $C/H$  ratio increases.

(h) The relative concentrations of  $C_nH_p$  with  $p = 6, 8$ , and 10 follow no obvious trend except that benzene is particularly prominent up to about 1500°K. As expected, its concentration is very high for high  $C/H$ . With regard to the relative concentrations of isomers, note that for the  $C_4H_4$  species vinyl acetylene reaches higher concentrations than does butatriene, even though the heat of formation of the former is approximately 4 kcal. higher than the latter. Evidently, the additional flexibility of the vinyl acetylene (internal rotation, etc.) favors this molecule entropywise. For the  $C_6H_4$  species, the same argument holds even though the chain isomers have heats of formation which are 8 kcal. higher than that of benzyne. The concentration of the latter is much smaller throughout the temperature range because of its stiffness and, therefore, lower entropy. In contrast, cyclopropane is always lower in concentration than the propene for two reasons; it has a higher heat of formation and a lower entropy.

(i) The temperature between 1500 and 2500°K. provides an interesting region for the use of single-pulse shock tubes for preparative purposes. The dominant species depends on the  $C/H$  ratio. If one starts with naturally occurring hydrocarbons which are rich in hydrogen, the first pass will lead to products which are carbon rich ( $C_2H_2$ ,  $C_6H_6$ , etc.) and hydrogen. A second pass of the resulting hydrocarbons will lead to a further carbon enrichment ( $C_4H_2$ ,  $C_6H_2$ , etc.). Of course, this hinges on the possibility of finding conditions which permit the attainment of this pseudo-equilibrium and quenching without excessive precipitation of carbon.

These computations need extension and further analysis. However, aside from the interesting new species which have to be considered in chain mechanisms, we have established a basis for selecting those species which are present in appreciable concentrations for the generation

of chains. Also, it is evident that the presence of many C/H fragments at equilibrium accounts for the product distributions observed for the quenched mixtures. One should not overlook the relative thermodynamic stabilities of the species and focus only on the kinetic routes by which conceivably they are generated. The emphasis should be on those elementary kinetic steps, which because of their low activation energies attain local equilibrium rapidly.

#### ACKNOWLEDGMENTS:

This work was supported in part by the Air Force (ARDC) under Contract AF33(616)-6694 and by the U. S. Atomic Energy Commission.

#### REFERENCES

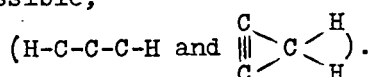
1. Ed., B. T. Brooks, et al., The Chemistry of Petroleum Hydrocarbons, Vol. II, Reinhold Publ. Co., New York, N. Y. (1955), refer to Chapter 22, E. W. R. Steacie and S. Bywater, and Chapter 25, L. Kramer and J. Happel.
2. A. G. Gaydon and H. G. Wolfhard, Flames, Their Structures, Radiations, and Temperatures, Chapman and Hall, Ltd., London (1953).
3. H. Tropsch and G. Egloff, Ind. Eng. Chem., **27**, 1063 (1935).
4. E. W. R. Steacie, Atomic and Free Radical Reactions, 2 vols., Reinhold Publ. Co., New York, N. Y. (1954).
5. A. F. Trotman-Dickenson, Gas Kinetics, Academic Press, Inc., New York, N. Y. (1955).
6. K. O. Kutschke and E. W. R. Steacie, Vistas in Free Radical Chemistry, Pergamon Press, London (1959).
7. Selections from chapters on Kinetics of Homogeneous Reactions, Annual Reviews of Physical Chemistry, Vols. I-X, Annual Reviews, Inc., Palo Alto (1950-59).
8. R. G. W. Norrish and B. A. Thrush, Quart. Rev., **X**, 149 (1956).
9. S. Claesson and L. Lindquist, Arkiv Kemi, **11**, 535, and **12**, 1 (1957).
10. N. H. Kiess and H. P. Broida, Seventh Symposium on Combustion, Butterworth Sci. Publ., London (1959), p. 207.
11. H. S. Glick, W. Squire, and A. Hertzberg, Fifth Symposium on Combustion, Reinhold Publ. Co., New York, N. Y. (1955), p. 393.
13. W. J. Hooker, Seventh Symposium on Combustion, loc cit, p. 949.
12. E. F. Greene, R. L. Taylor, and W. L. Patterson, Jr., J. Phys. Chem., **62**, 238 (1958).
14. H. S. Glick, Seventh Symposium on Combustion, loc cit, p. 98.
15. G. B. Kistiakowsky, private communication.
16. G. B. Skinner and R. A. Ruehrwein, J. Phys. Chem., **63**, 1736 (1959).
17. V. Kevorkian, C. E. Heath, and M. Boudart, ibid, **64**, 695 (1960).
18. G. B. Skinner and W. E. Ball, ibid, **64**, 1025 (1960).
19. G. B. Skinner and E. M. Sokoloski, ibid, **64**, 1028 (1960).
20. L. S. Kassel, J. Am. Chem. Soc., **54**, 3949 (1932).
21. A. Shepp, J. Chem. Phys., **24**, 939 (1956).
22. S. H. Bauer, et al., WADD Tech. Report 60-107 (April, 1960).
23. G. B. Kistiakowsky and W. G. Zinman, J. Chem. Phys., **23**, 1889 (1955).
24. Ed., Y. S. Touloukian, Thermodynamic and Transport Properties of Gases, Liquids, and Solids, McGraw-Hill, New York, N. Y. (1959), article by H. Kroepelin and E. Winter, p. 438.

25. M. N. Flooster and T. R. Reed, J. Chem. Phys., 31, 66 (1959).
26. D. A. Ramsay, Annals N. Y. Acad. Sci., 67, 485 (1957); J. H. Collomon and D. A. Ramsay, Can. J. Phys., 35, 129 (1957).
27. C. C. Costain and B. P. Stoicheff, J. Chem. Phys., 30, 777 (1959).
28. L. R. Sitney, PUBCO-I for Computing the Ideal Thermodynamic Functions of a Polyatomic Gas Molecule, LA-2278, issued May 8, 1959, by LASL.

# FOOTNOTES TO TABLE I

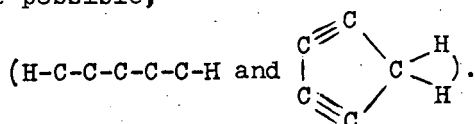
<sup>a</sup> A few species were not considered in detail:  $C_2H_5$ ,  $C_3H_7$ ,  $C_4H_7$ ,  $C_4H_9$ ,  $H_3C-C\equiv C$ ,  $HC=CH-CH_2$ ,  $H_2C=CH-C\equiv C$ ,  $H_2C-HC=CH-CH_2$ , and a variety of cyclic structures in which there is incorporated large amounts of bond-angle strain energy. Rough estimates indicated that either the heats of formation of these species were considerably larger than those of their isomers which were included or that their entropies were considerably smaller than that of the products into which they could readily dissociate.

<sup>b</sup> Two isomers are possible,



The estimate cited was made for the linear species, but a rough analysis shows that the heat of formation of the cyclic compound will be rather close to that of the chain.


<sup>c</sup> Two isomers are possible,



The estimate cited was made for the linear species, but a rough analysis shows that the heat of formation of the cyclic compound will be rather close to that of the chain.

TABLE I

C/H Species Included in Revised Computation and Their Heats of Formation ( $\Delta H_f^\circ$ )<sup>a</sup>

H	(51.62)	O <sub>2</sub>	(198)	O <sub>3</sub>	(189)	O <sub>4</sub>	(238.5)	C <sub>5</sub>	(237)	O <sub>6</sub>	[287]
H <sub>2</sub>		O <sub>2</sub> H	[116.7]	O <sub>3</sub> H	[127.1]	O <sub>4</sub> H	[154]	O <sub>5</sub> H	[185.4]	O <sub>6</sub> H	[211.3]
		C <sub>2</sub> H <sub>2</sub>	(54.33)	C <sub>3</sub> H <sub>2</sub>	[106.7]	C <sub>4</sub> H <sub>2</sub>	(111.3)	O <sub>6</sub> H <sub>2</sub>	[165]	C <sub>6</sub> H <sub>2</sub>	[168.6]
O <sub>2</sub> H <sub>3</sub>	(66.9)	H <sub>2</sub> C-O $\equiv$ CH	(77.3)	H <sub>2</sub> C-O-O $\equiv$ CH		H <sub>2</sub> C-O-O $\equiv$ CH	[102.5]	C <sub>5</sub> H <sub>3</sub>	[135.6]	O <sub>6</sub> H <sub>3</sub>	[158.3]
O <sub>2</sub> H <sub>4</sub>	(14.52)	H <sub>3</sub> C-O $\equiv$ CH	(46.017)	H <sub>3</sub> C-O-O $\equiv$ CH <sub>2</sub>		H <sub>3</sub> C-O-O $\equiv$ CH <sub>2</sub>	[71.3]	HC $\equiv$ C-O $\equiv$ C-CH <sub>3</sub>	(103.6)	H <sub>2</sub> C-(C) <sub>3</sub> -C $\equiv$ CH	[132]
CH	[140.4]	H <sub>2</sub> C-O-O $\equiv$ CH <sub>2</sub>	(47.70)	H <sub>2</sub> C-O-O $\equiv$ CH		H <sub>2</sub> C-O-O $\equiv$ CH	(75.3)	H <sub>2</sub> C-O-O $\equiv$ CH-O $\equiv$ CH	[108.3]	H <sub>2</sub> C-(C) <sub>4</sub> -CH <sub>2</sub>	[132.8]
CH <sub>2</sub>	(66.8)	H <sub>2</sub> C-OH-CH <sub>2</sub> [35]		H <sub>3</sub> C-C $\equiv$ C-CH <sub>2</sub>		H <sub>3</sub> C-C $\equiv$ C-CH <sub>2</sub>	[67.8]	H <sub>2</sub> C-O-C $\equiv$ C-CH <sub>2</sub>	[102.3]		[124]
CH <sub>3</sub>	(33.4)			H <sub>2</sub> C-OH-O-CH <sub>2</sub>		H <sub>2</sub> C-OH-O-CH <sub>2</sub>	[67.1]				
CH <sub>4</sub>	(-15.99)										
		O <sub>2</sub> H <sub>6</sub>	(-16.517)	H <sub>3</sub> C-OH-CH <sub>2</sub>	(8.468)	H <sub>2</sub> C-OH-CH-CH <sub>2</sub>	(29.78)	HC=CH-CH <sub>2</sub>	(25.2)	(CH) <sub>6</sub>	(24.0)
		(CH <sub>2</sub> ) <sub>3</sub>	(17.8)	(H <sub>3</sub> C-O $\equiv$ ) <sub>2</sub>		(H <sub>3</sub> C-O $\equiv$ ) <sub>2</sub>	(38.09)				
				H <sub>3</sub> C-OH-C-CH <sub>2</sub>		H <sub>3</sub> C-OH-C-CH <sub>2</sub>	(42.00)				
				H <sub>3</sub> C <sub>2</sub> -C $\equiv$ CH		H <sub>3</sub> C <sub>2</sub> -C $\equiv$ CH	(42.74)				
		O <sub>3</sub> H <sub>8</sub>	(-19.482)	(CH <sub>2</sub> ) <sub>4</sub>		(CH <sub>2</sub> ) <sub>4</sub>	(12.5)				
				O <sub>4</sub> H <sub>8</sub> (isomers)		O <sub>4</sub> H <sub>8</sub> (isomers)	{(3.48) (0.98)}				
							{(4.96) (2.24)}				
				C <sub>4</sub> H <sub>10</sub> (isomers)		C <sub>4</sub> H <sub>10</sub> (isomers)	(-23.67)				
							(-25.30)				

( ) values deduced in a rather direct manner from experiment

[ ] estimated by analogy, etc.

C <sub>7</sub>	[287]	C <sub>8</sub>	[339]	C <sub>9</sub>	[334]	O <sub>10</sub>	[393]
C <sub>7</sub> H	[240]	C <sub>8</sub> H	[267]	C <sub>9</sub> H	[291]	C <sub>10</sub> H	[324]
C <sub>7</sub> H <sub>2</sub>	[220]	C <sub>8</sub> H <sub>2</sub>	[225]	C <sub>9</sub> H <sub>2</sub>	[271]	C <sub>10</sub> H <sub>2</sub>	[282]



TABLE II

Compound	Process	$\Delta H_{\text{of}}^{\circ}$ (kcal.)	Compound	Process	$\Delta H_{\text{of}}^{\circ}$ (kcal.)
$\begin{array}{c} \text{H} & & \text{H} \\ & \diagdown & / \\ & \text{C}=\text{C}=\text{C} \\ & / & \diagdown \\ \text{H} & & \text{Me} \end{array}$	1 + 2	65.7		1 + 2 + 3 + 4	104.1
	8 + 2	66.6		1 + 2 + 3a + 4a	100.7
	Heat of hydrogenation	66.5		8 + 2 + 3 + 4	105.0
$\begin{array}{c} \text{H} & & \text{H} \\ & \diagdown & / \\ & \text{C}=\text{C} \\ & / & \diagdown \\ \text{H} & & \text{C}\equiv\text{C}-\text{Me} \end{array}$	1 + 5	65.5	$\begin{array}{c} \text{H} & & \text{H} \\ & \diagdown & / \\ & \text{C}=\text{C}=\text{C}=\text{O} \\ & / & \diagdown \\ \text{H} & & \text{H} \end{array}$	8 + 2 + 3a + 4a	101.6
	8 + 5	66.4		8 + 5 + 6 + 4	101.8
	Heat of hydrogenation	66.4		8 + 5 + 9 + 10	101.8
	11 + 12	63.2		1 + 5 + 9 + 10	100.9
$\begin{array}{c} \text{H} & & \text{H} \\ & \diagdown & / \\ & \text{C}=\text{C}=\text{C} \\ & / & \diagdown \\ \text{H} & & \text{H} \end{array}$	11a + 12a	63.3		11 + 12 + 13 + 10	102.7
	Heat of hydrogenation	62.5		11 + 12 + 14 + 15	101.8
$\begin{array}{c} \text{H} & & \text{H} \\ & \diagdown & / \\ & \text{C}=\text{C}=\text{C} \\ & / & \diagdown \\ \text{H} & & \text{H} \end{array}$	1 + 2 + 3a	96.5	$\text{MeC}\equiv\text{C}-\text{C}\equiv\text{CH}$	1 + 2 + 3 + 7	104.8
	8 + 2 + 3a	97.4		1 + 5 + 6 + 7	101.6
	1 + 5 + 9	96.7		8 + 2 + 3 + 7	105.7
	11 + 12 + 13	98.5		8 + 5 + 6 + 7	102.5
$\begin{array}{c} \text{H} & & \text{H} \\ & \diagdown & / \\ & \text{C}=\text{C}=\text{C} \\ & / & \diagdown \\ \text{H} & & \text{H} \end{array}$			$\begin{array}{c} \text{H} & & \text{H} \\ & \diagdown & / \\ & \text{C}=\text{C}=\text{C} \\ & / & \diagdown \\ \text{H} & & \text{H} \end{array}$	11 + 12 + 14 + 16	108.7
				Heat of hydrogenation	107.9

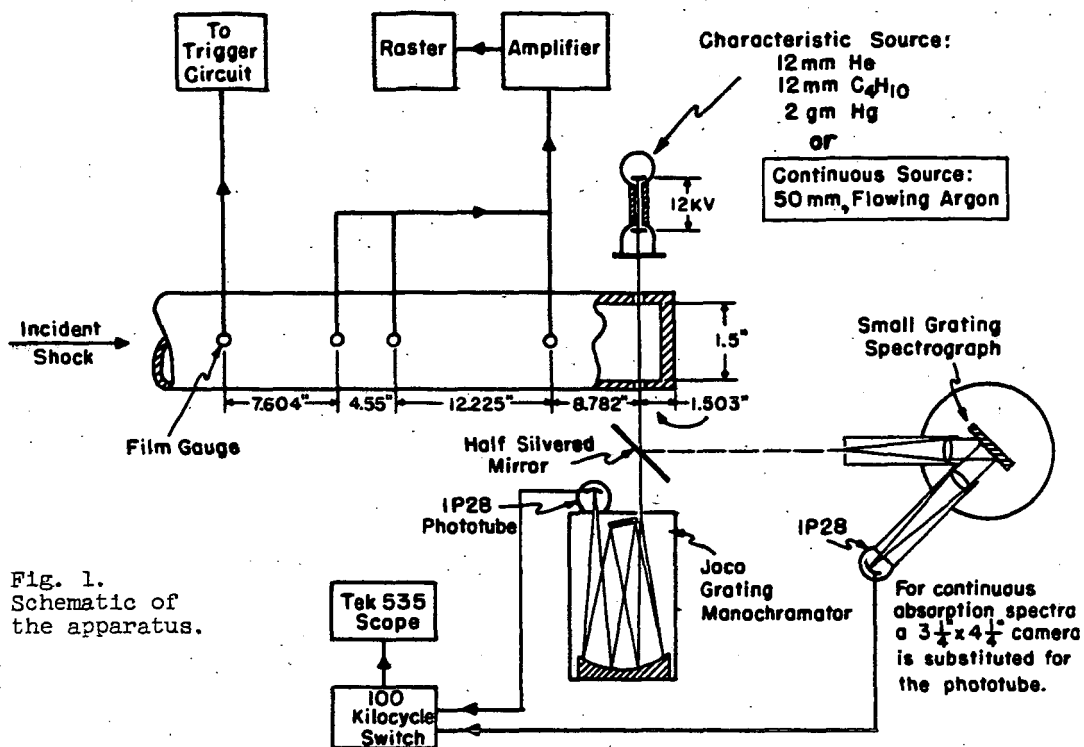
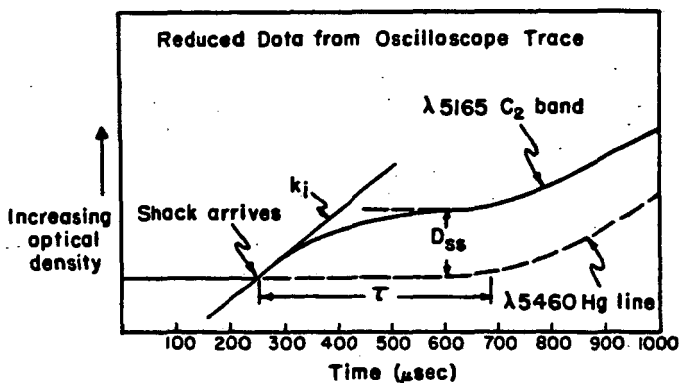


Fig. 1.  
Schematic of  
the apparatus.



$\tau$  = Induction period  
 $D_{ss}$  = Steady state  $C_2$  conc.  
 $k_i$  = Initial rate constant for formation of  $C_2$

Fig. 2.

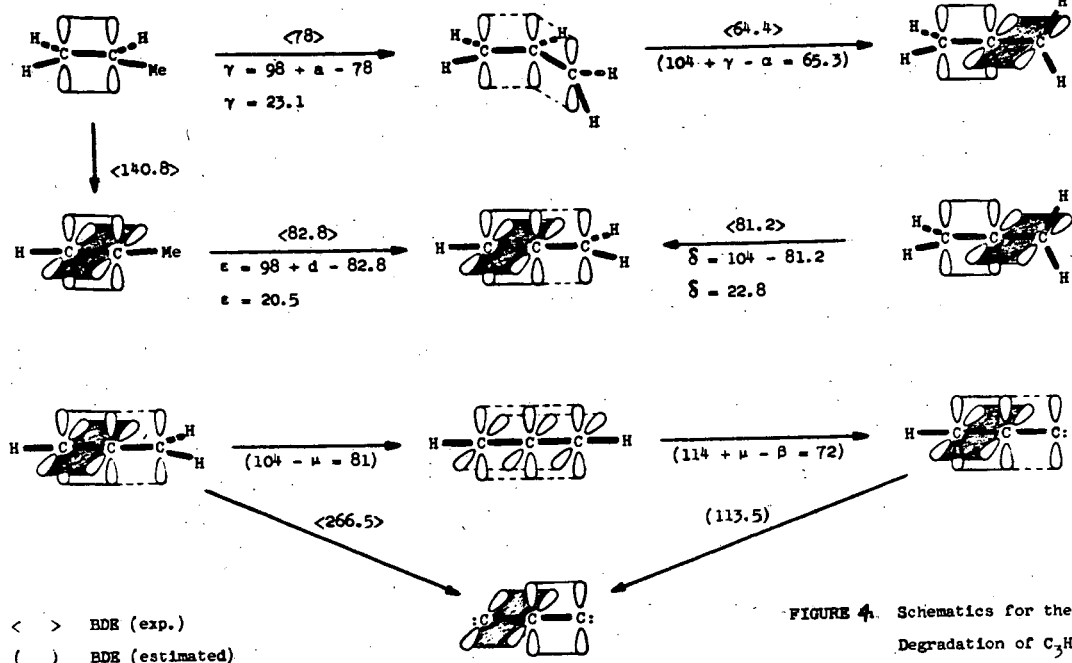


FIGURE 4. Schematics for the Degradation of  $C_3H_6$

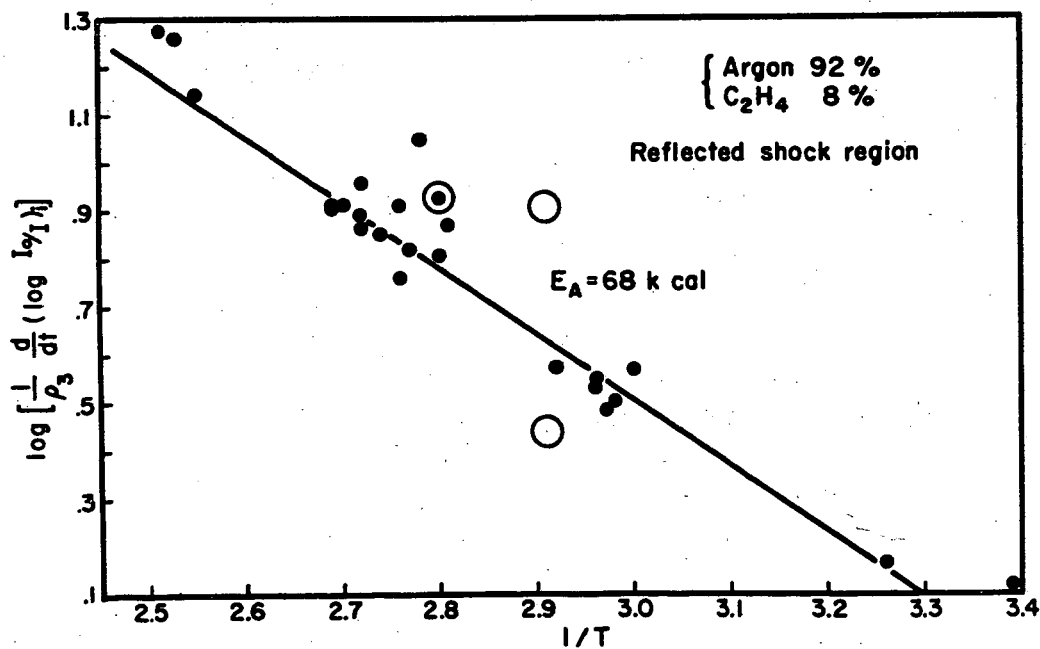


Fig. 3. Activation Energy for the Production of  $C_2$

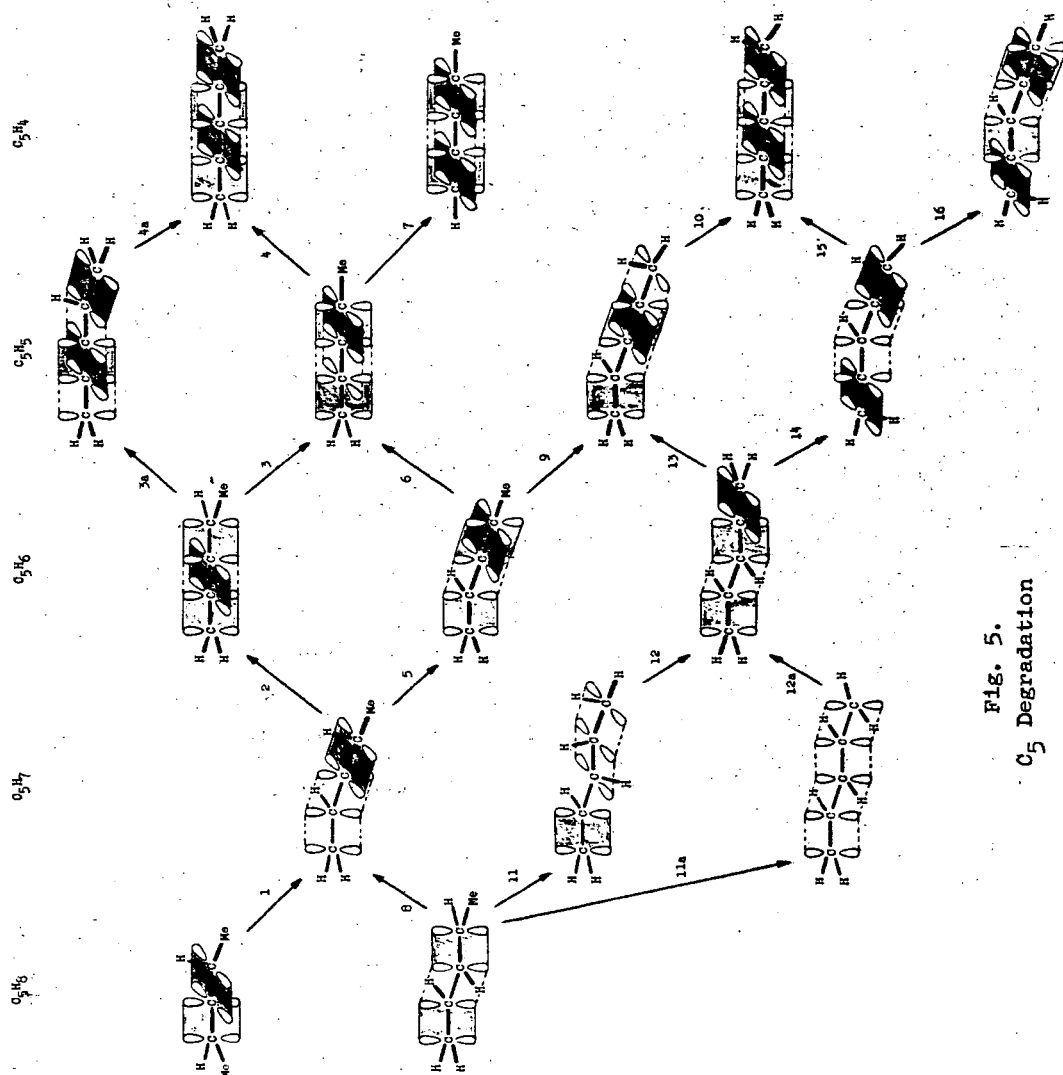


Fig. 5.  
 $C_5$  Degradation

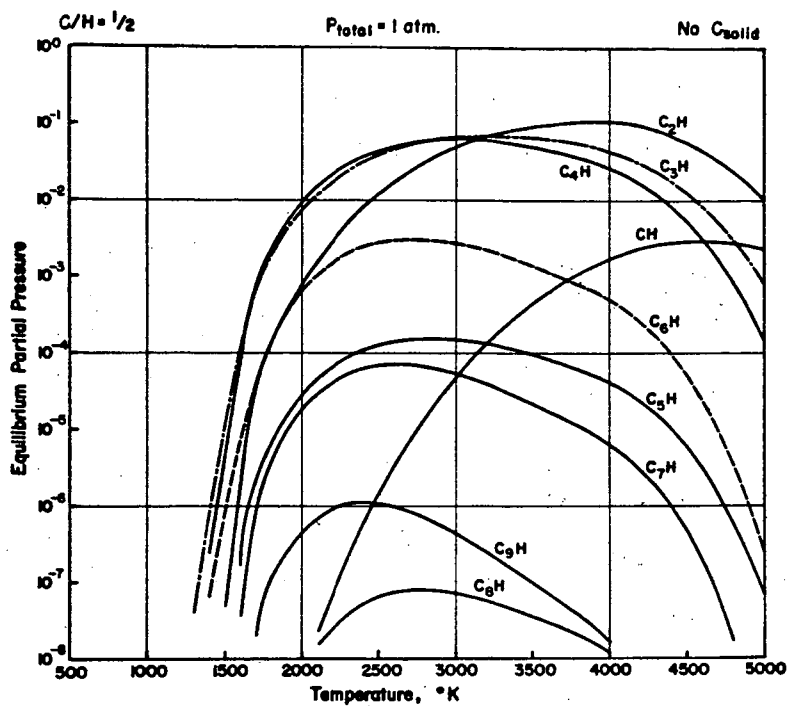


Fig. 6.

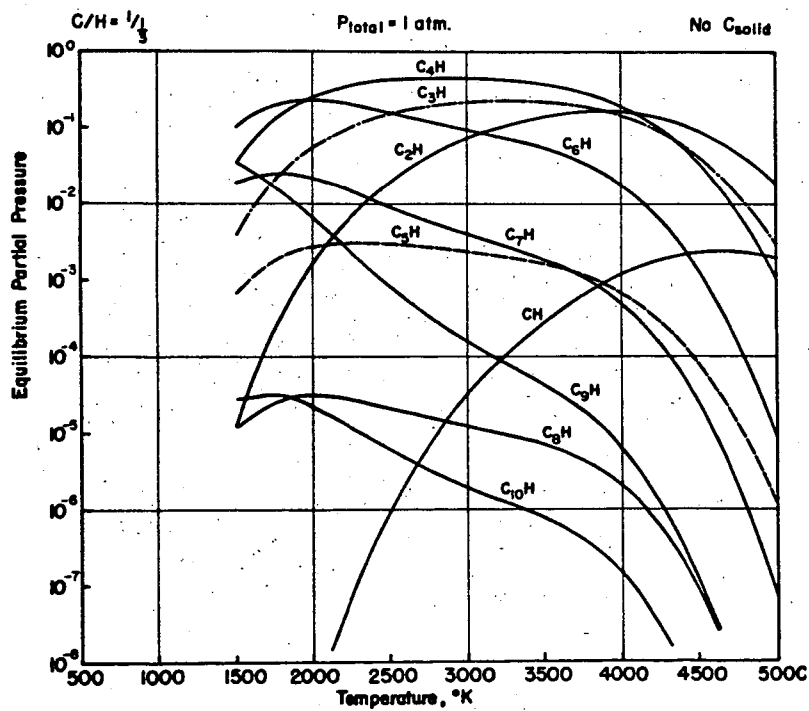


Fig. 7.

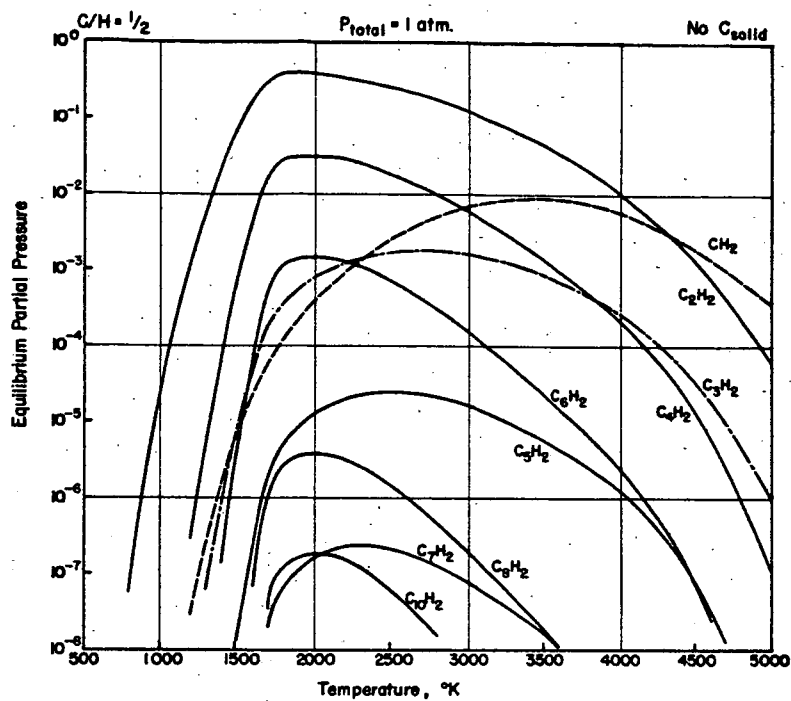


Fig. 8.

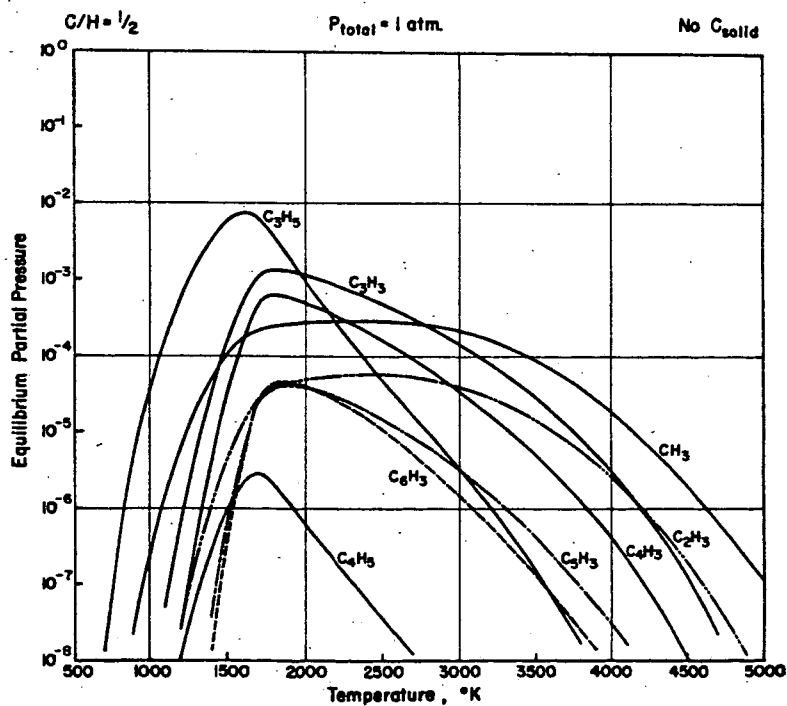


Fig. 9.

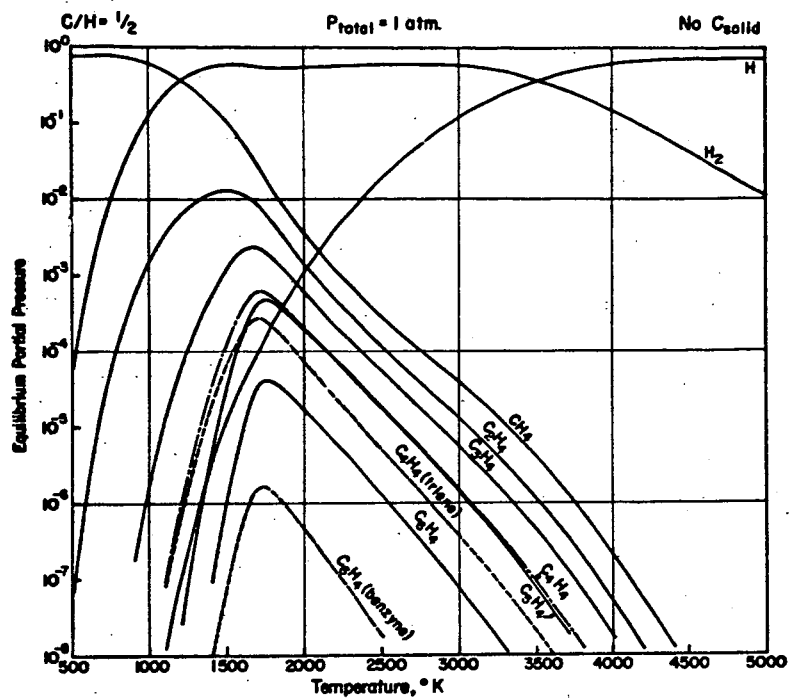


Fig. 10.

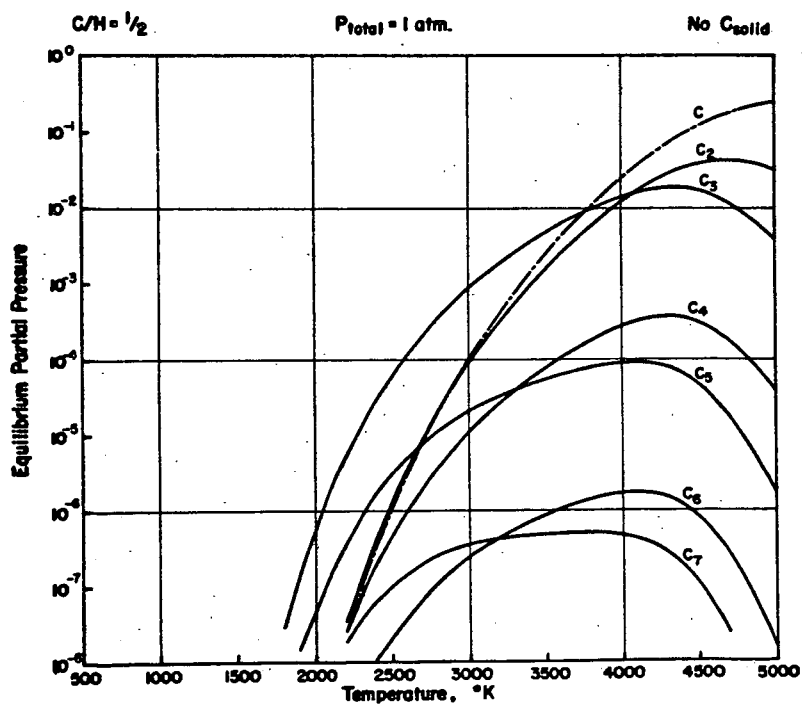


Fig. 11.

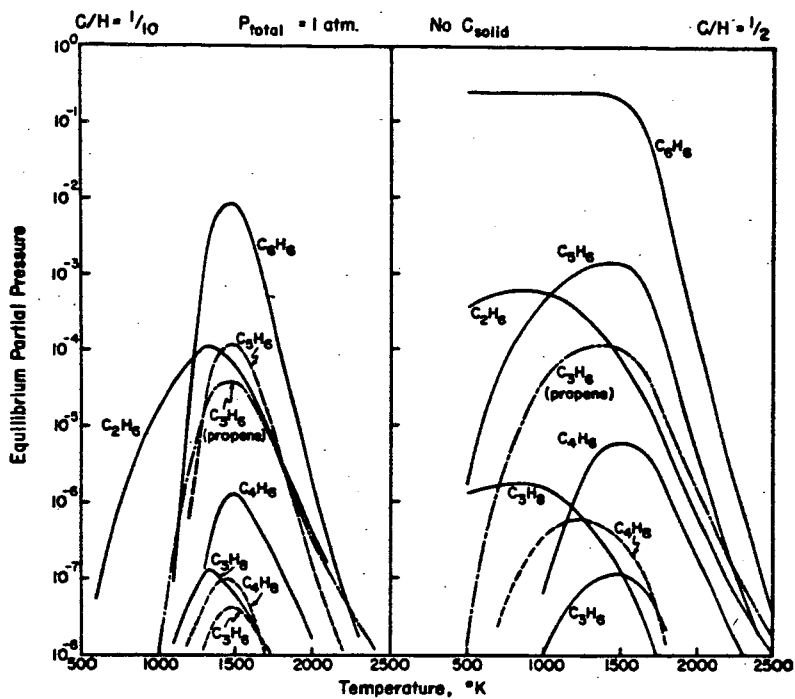


Fig. 12.

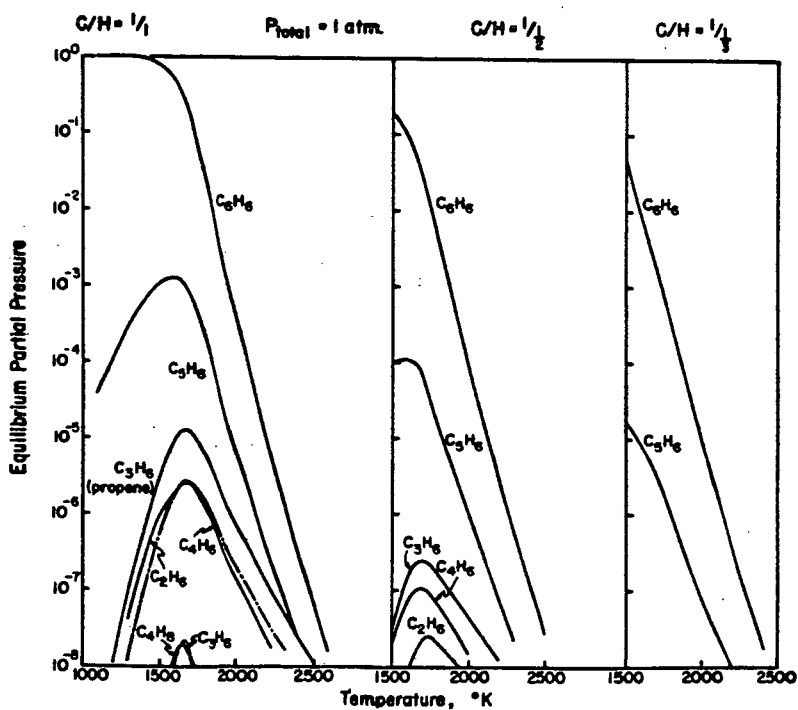


Fig. 13.